March 4, 2020
Volume 142
Number 9
pubs.acs.org/JACS

JACS

JOURNAL OF THE AMERICAN CHEMICAL SOCIETY

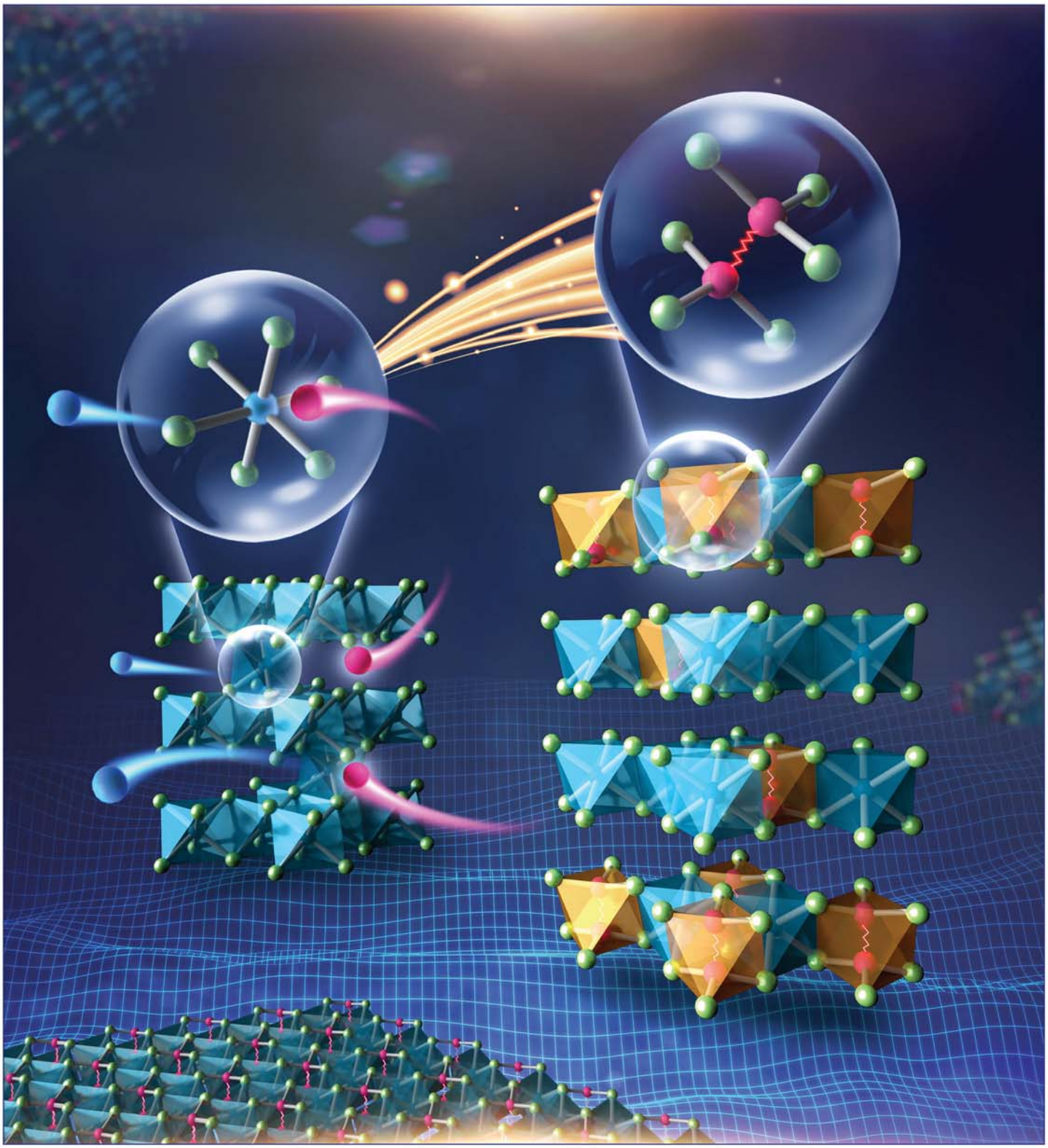

ACS Publications
Most Trusted. Most Cited. Most Read.

www.acs.org

JACS
JOURNAL OF THE AMERICAN CHEMICAL SOCIETY
pubs.acs.org/JACS
Article

Solution Synthesis of Layered van der Waals (vdW) Ferromagnetic $CrGeTe_3$ Nanosheets from a Non-vdW Cr_2Te_3 Template

Huan Yang, Fang Wang,* Huisheng Zhang, Lihong Guo, Liyan Hu, Lanfang Wang, Ding-Jiang Xue,* and Xiaohong Xu*

Cite This: J. Am. Chem. Soc. 2020, 142, 4438−4444
Read Online
ACCESS | Metrics & More | Article Recommendations | Supporting Information

ABSTRACT: $CrGeTe_3$ has recently emerged as a new class of two-dimensional (2D) materials due to its intrinsic long-range ferromagnetic order. However, almost all the reported synthesis methods for $CrGeTe_3$ nanosheets are based on the conventional mechanical exfoliation from single-crystalline $CrGeTe_3$, which is prepared by the complicated self-flux technique. Here we report a solution-processed synthesis of $CrGeTe_3$ nanosheets from a non-van der Waals (vdW) Cr_2Te_3 template. This structure evolution from non-vdW to vdW is originated from the substitution of Ge atoms on the Cr sites surrounded by fewer Te atoms in the Cr_2Te_3 lattice due to their smaller steric hindrance and lower energy barrier. These $CrGeTe_3$ nanosheets present regular hexagonal structures with a diameter larger than 1 μm and excellent stability. They exhibit soft magnetic behavior with a Curie temperature lower than 67.5 K. This non-vdW to vdW synthesis strategy promotes the development of $CrGeTe_3$ in ferromagnetism while providing an effective route to synthesize other 2D materials.

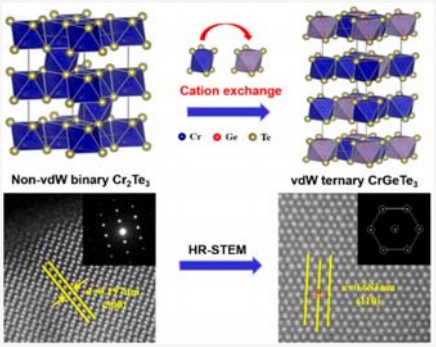

1. INTRODUCTION

The lack of ferromagnetism in conventional two-dimensional (2D) materials has limited their developments and applications in spintronic devices.[1−6] The extrinsic ferromagnetism introduced by regulating the strain, edge structure, or defects is usually hard to control in 2D materials.[7−10] It is necessary to explore the novel 2D materials with an intrinsic long-range ferromagnetism. $CrGeTe_3$ has recently emerged as a very promising candidate material due to its intrinsic characteristics of both semiconductor and ferromagnetism.[11−15] $CrGeTe_3$ is a substantially 2D layered transition-metal chalcogenide (TMD). These layers are stacked together via the van der Waals (vdW) interaction with an interlayer distance of 6.9 Å.[16−18] The ferromagnetic order in bilayer $CrGeTe_3$ was first found by Gong et al. in 2017.[15] This study indicated that the ferromagnetism can be inherited as the thickness is thinner than several atomic layers; the long-range ferromagnetic interaction can be easily achieved in $CrGeTe_3$ nanosheets. The emergence of ferromagnetism in $CrGeTe_3$ opens vast opportunities for 2D materials in magnetic, magnetoelectric, and magneto-optic applications.[19−24]

Driven by the fascinating properties of $CrGeTe_3$ and its promising applications in flexible devices, great efforts have been devoted to produce ultrathin 2D $CrGeTe_3$ nanomaterials. The mechanical exfoliation method has been widely used to obtain monolayer or multiple-layer $CrGeTe_3$ nanoflakes by breaking the weak vdW interaction between the layers in single-crystalline $CrGeTe_3$.[15−17,20] The single crystal used in this method is usually prepared by the self-flux technique.[15,17,19,20] Such a method usually needs a long period and an ultrahigh temperature, even higher than 1000 °C.[17,19] Moreover, the yield of mechanical exfoliation is very low. Therefore, it is highly desirable to develop a facile and feasible method for the preparation of 2D $CrGeTe_3$ nanosheets.

Here we propose a solution synthesis of 2D $CrGeTe_3$ nanosheets through a chemical cation exchange method. The first-principles calculation reveals the non-vdW Cr_2Te_3 template can be completely evolved to vdW $CrGeTe_3$ when some Cr sites of the Cr_2Te_3 lattice are exchanged with Ge sites. The key point for this exchange is the Cr sites in the Cr_2Te_3 lattice surrounded by fewer Te atoms having a smaller steric hindrance and lower energy barrier. Based on the theoretical design, we successfully obtained the ferromagnetic $CrGeTe_3$ nanosheets with uniform hexagonal morphology larger than 1 μm. The phase structures and magnetic properties in the synthesis process were systematically investigated through related structural and magnetic characterizations. This non-vdW to vdW evolution strategy is expected to be a new method to obtain other ternary 2D materials.

Received: December 15, 2019
Published: January 24, 2020

https://dx.doi.org/10.1021/jacs.9b13492
J. Am. Chem. Soc. 2020, 142, 4438−4444

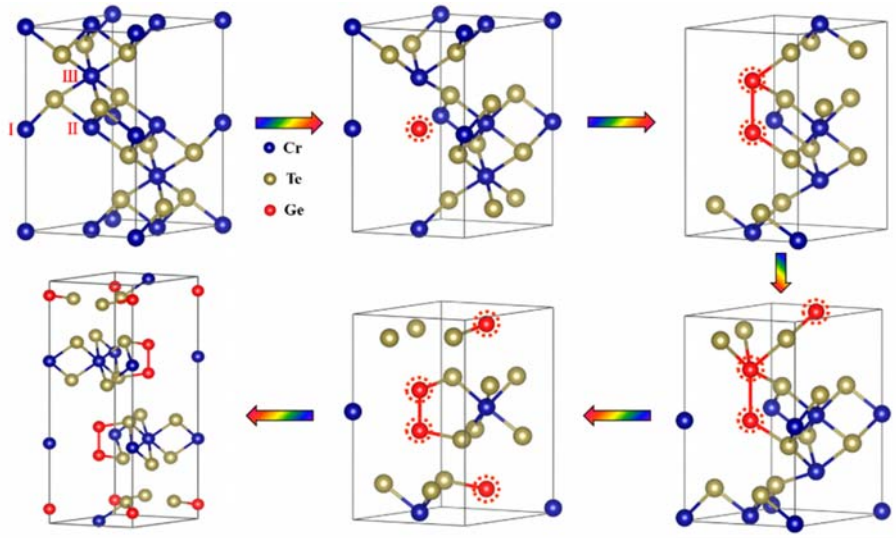

Figure 1. Schematic illustration of the theoretical simulation from non-vdW Cr_2Te_3 to vdW $CrGeTe_3$.

2. EXPERIMENTAL SECTION

2.1. Theoretical Simulations. The first-principles calculations were performed to simulate the transition process from Cr_2Te_3 to $CrGeTe_3$. Here, the electronic structures of Cr_2Te_3 and Ge-introduced Cr_2Te_3 were calculated by using the projector augmented wave (PAW) formalism in the Vienna *ab initio* simulation package (VASP).[25,26] The Perdew–Burke–Ernzerhof (PBE) approximation was used to describe the exchange and correlation functional. The plane-wave cutoff energy was set to 400 eV. All the atoms in the supercells were allowed to move until the Hellmann–Feynman force on each atom was smaller than 0.01 eV/Å. The gamma-centered Monkhorst–Pack *k*-point meshes of 9 × 9 × 5 were adopted in all calculations. The vdW correction with the Grimme (DFT-D2) method was included in all calculations.[27]

2.2. Chemicals. Hexacarbonyl chromium ($Cr(CO)_6$, 99%), tellurium powder (Te, 200 mesh, 99.999%), and germanium(IV) chloride (GeI_4, 99.9999%) were purchased from Alfa Aesar. Oleylamine (OLA, 80–90%, boiling point 350 °C) and trioctylphosphine (TOP, 90%) were obtained from Aladdin and Energy Chemical, respectively. Hexane (99.5%) and ethanol (99.7%) were purchased from Tianjin Kermel and Guangfu. All the chemicals were used as received, without further purification.

2.3. Synthesis. The $CrGeTe_3$ nanostructure was obtained by a two-step synthesis procedure. First, a Cr_2Te_3 binary template was synthesized by a modified organic-solvent-phase chemical decomposition method.[28] The source ratio of Cr:Te was 1:1.8. Second, the ternary $CrGeTe_3$ was prepared by injecting a Ge source into a binary Cr_2Te_3 seed crystal using the cation exchange method.

The Cr_2Te_3 seed crystal suspension (1 mmol) was dispersed in a flask with 30 mL of OLA. The system was then pumped down with a flow of nitrogen at room temperature for 30 min to remove the low-boiling-point solvent and oxygen. The clear colorless solution of 1 mmol of GeI_4 dissolved in 5 mL of OLA was injected into the mixture solution dropwise at 100 °C under vigorous stirring. Subsequently, when the temperature went to the reflux temperature of 330 °C at a heating rate of 5 °C/min, the reaction mixture was stirred for 2 h at this temperature. After the reaction, the solution was rapidly cooled to room temperature, and the extraction purification procedure was similar to that of Cr_2Te_3. The $CrGeTe_3$ nanostructure could be dispersed in hexane.

2.4. Characterization. The phase structures and element valences were characterized by powder X-ray diffraction (XRD) with a Cu Kα radiation source (λ = 0.154 nm) and an X-ray photoelectron spectrometer (XPS). The morphologies were obtained using transmission electron microscopy (TEM). High-resolution TEM (HRTEM) images, high-angle annular dark field scanning TEM (HAADF-STEM) images, high-resolution scanning TEM (HR-STEM) images, and selected area electron diffraction (SAED) patterns were collected using scanning TEM equipped with spherical aberration correctors on the image. The magnetic measurements including the magnetic hysteresis (M–H) loops and magnetization–temperature (M–T) curves were performed using a physical property measurement system. The thickness of the nanosheets was characterized by scanning electron microscope (SEM) and atomic force microscope (AFM). The composition of the solution was characterized by inductively coupled plasma atomic emission spectroscopy (ICP-AES). The organic ligands were investigated by using a Fourier transform infrared spectrometer (FT-IR).

3. RESULTS AND DISCUSSION

We begin with a comparison of the crystal lattices of Cr_2Te_3 and $CrGeTe_3$. Cr_2Te_3 is a three-dimensional hexagonal structure with a $P\bar{3}1c$ (No. 163) space group (a = 6.82 Å, c = 12.08 Å) (Figure S1).[28] In this nonlayered Cr_2Te_3 unit cell, there are three types of Cr atoms: one-quarter of the Cr atoms occupy the Cr_I site, one-half occupy the Cr_{II} site, and others occupy the Cr_{III} site. In contrast, the $CrGeTe_3$ is a substantial 2D layered lattice with a large interlayer gap (d_0 = 6.9 Å), which has a similar hexagonal structure with an $R\bar{3}$ (No. 148) space group (a = 6.83 Å, c = 20.56 Å).[16,17] Based on the above comparison, we took the view that the conversion from nonlayered binary Cr_2Te_3 to layered ternary $CrGeTe_3$ may be easy to realize if all of the Cr_{III} and one-half of the Cr_{II} sites in Cr_2Te_3 are substituted with Ge atoms by breaking the interlayer Cr–Te ionic bonds (Figure S1).

First-principles calculations were then performed to reveal the probability of the evolution from non-vdW Cr_2Te_3 to vdW $CrGeTe_3$ through transformation energy. The total energies of Ge-introduced Cr_2Te_3 with different configurations were systematically investigated. Several configurations were considered for each Ge-introduced Cr_2Te_3 system in our calculations (Figure S2), and the most stable configurations are displayed in Figure 1. The substitution process can be well understood by the following steps: (i) when one Ge atom is introduced to the primitive Cr_2Te_3 (Figure S2), the Ge atom tends to replace the Cr_{II} site (E = −119.114 eV) rather than the Cr_{III} site (E = −118.898 eV). This can be attributed to the

https://dx.doi.org/10.1021/jacs.9b13492
J. Am. Chem. Soc. 2020, 142, 4438–4444

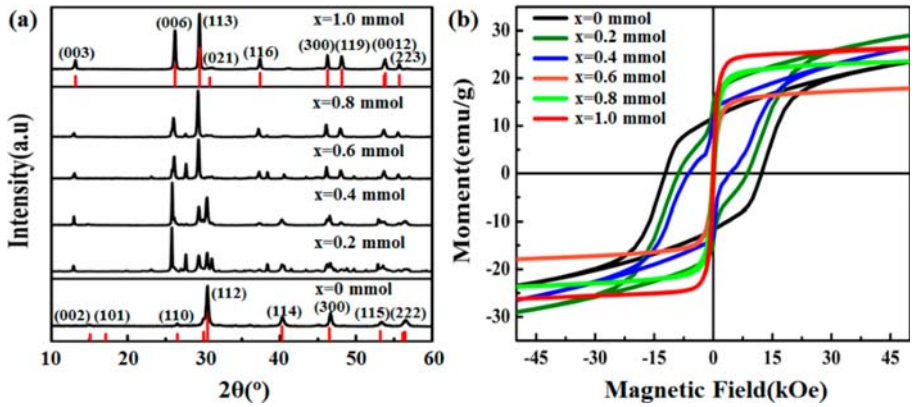

Figure 2. (a) XRD patterns and (b) $M-H$ loops (measured at 5 K) of Ge-doped Cr_2Te_3 samples with different Ge contents.

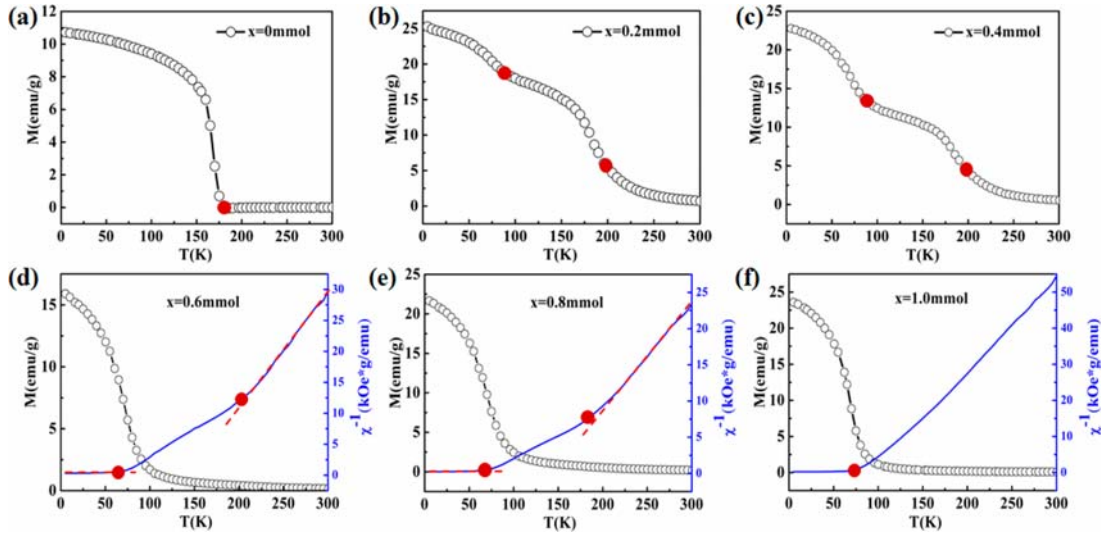

Figure 3. $M-T$ curves of Ge-doped Cr_2Te_3 samples with different Ge contents (H_{appl} = 5 kOe). The $1/\chi = T$ curves (blue solid lines) are fitted according to the Curie–Weiss law.

large steric hindrance and high energy barrier for the substitution of the Cr_{III} site, which is surrounded by six Te atoms. (ii) When another Ge atom is introduced, it favors the replacement of the Cr_{III} site, subsequently forming a chemical bond between the two Ge atoms (E = −113.479 eV). The substitution of the Cr_{III} site would break the connection between the layers, resulting in the delamination phenomenon and the evolution from non-vdW Cr_2Te_3 to vdW $CrGeTe_3$. Hence, the incomplete Ge substitution in the Cr_2Te_3 lattice would lead to the separate existence of Cr_2Te_3 and $CrGeTe_3$ phases. This means that it is impossible to form the transition state of $Cr_{2-x}Ge_xTe_3$ in the reaction process. (iii) Similarly, if more Ge atoms are introduced, steps (I) and (II) will be repeated. Finally, when half of the Cr atoms are substituted by Ge atoms, the Ge-doped Cr_2Te_3 will become $CrGeTe_3$.

To evaluate this cation exchange strategy from experiment, we first prepared the Cr_2Te_3 template according to previous work. The cation exchange reaction is usually used to synthesize multiple nanostructures or heterojunctions.[29−31] This process was then precisely regulated through the content of the GeI_4 precursor with the Cr_2Te_3 template. The XRD patterns of the samples with different Ge contents ($0 \le x \le 1$ mmol) are shown in Figure 2a. When x = 0 mmol, all the diffraction peaks are consistent with the Cr_2Te_3 standard pattern (JCPDS: 29-0458), indicating the pure phase of the Cr_2Te_3 template. Note that the $CrGeTe_3$ crystal phase appears in the sample of x = 0.2 mmol. The (003), (006), and (113) diffraction peaks of $CrGeTe_3$ begin to be observed at 2θ = 12.91°, 25.99°, and 29.20°, while the main peaks of Cr_2Te_3 still exist. This shows that Cr_2Te_3 and $CrGeTe_3$ coexist in the system by a partial replacement of Cr^{3+} with Ge^{4+}. The main peaks of $CrGeTe_3$ become stronger with an increasing content of Ge source. The pure $CrGeTe_3$ phase (JCPDS: 50-0928) without any other impurities is acquired when x = 1.0 mmol. This reveals that half of the Cr^{3+} cations in Cr_2Te_3 have been completely substituted by Ge^{4+} to form $CrGeTe_3$. Briefly, the XRD results show that the binary Cr_2Te_3 can be successfully transformed to ternary $CrGeTe_3$ through the cation exchange process, agreeing well with our calculation results.

Now we further investigate the cation exchange process through the characterization of magnetic behavior. It has been reported that Cr_2Te_3 shows hard magnetic behavior,[28] while $CrGeTe_3$ exhibits soft magnetic behavior.[15,19] The soft/hard exchange coupled interaction should exist if the phases of Cr_2Te_3 and $CrGeTe_3$ coexist during the cation exchange process. Figure 2b shows the magnetic hysteresis loops ($M-H$,

https://dx.doi.org/10.1021/jacs.9b13492
J. Am. Chem. Soc. 2020, 142, 4438−4444

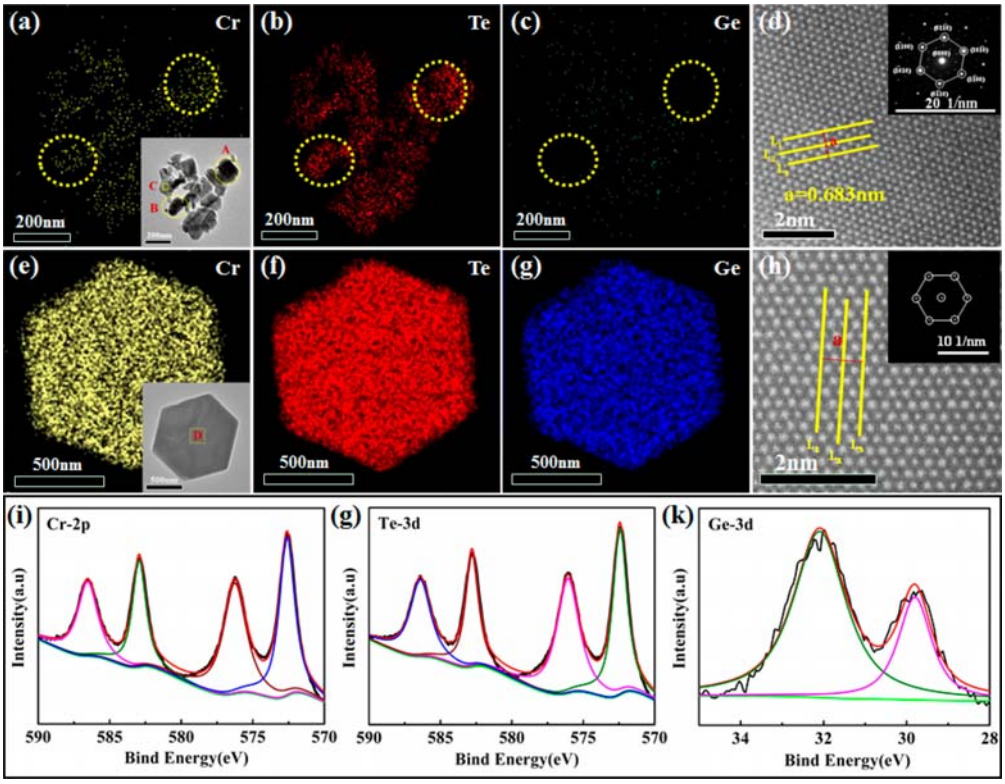

Figure 4. Typical TEM elemental mapping of Cr, Te, and Ge in samples of x = 0.4 mmol (a–c) and x = 1.0 mmol (e–g), HR-STEM image and SAED pattern of regions C and D (d, h), and high-resolution XPS survey of Cr 2p, Te 3d, and Ge 3d for the $CrGeTe_3$ nanosheets (i–k).

5 K) of samples with different Ge contents. The coercivity (H_c) of the pure Cr_2Te_3 reaches 13 kOe, exhibiting a hard magnetic behavior. When x = 0.2 mmol, H_c decreases to 8.6 kOe, and a clear kink appears close to the zero field. It indicates that there exists a soft magnetic $CrGeTe_3$ phase in the sample in addition to the hard magnetic Cr_2Te_3, in agreement with the XRD results (Figure 2a). A similar result can be found in the case of x = 0.4 mmol. Nevertheless, only the soft magnetic behaviors are observed in the samples of 0.6 mmol $\leq x \leq$ 1 mmol, and the saturation magnetization (M_s) gradually increases as the GeI_4 precursor increases. An M_s of 25.6 emu/g is obtained for the pure-phase $CrGeTe_3$ (x = 1.0 mmol), close to the values reported previously.[19] The H_c value is only 155 Oe for pure $CrGeTe_3$, indicating an obvious soft magnetic behavior. The enhancement of the $CrGeTe_3$ main phase results in the decrease of the Cr_2Te_3 hard magnetic phase. The transformation from hard to soft is related closely with this chemical reaction process from Cr_2Te_3 to $CrGeTe_3$, confirming our XRD results.

To further confirm the coexistence of the Cr_2Te_3 and $CrGeTe_3$ phases, the temperature dependence of magnetization $M(T)$ of the samples with different Ge contents was measured under H = 5 kOe. A sharp transition occurs between 175 and 180 K (Figure 3a). This means that the Curie temperature (T_c) of Cr_2Te_3 is approximately 180 K, in accord with our reported results.[28] Nevertheless, two obvious transitions appear in Figure 3b (x = 0.2 mmol) and Figure 3c (x = 0.4 mmol), indicating the mixture phases coexist at these stages. Therefore, combined with the XRD and M–H results, the mixture phases are confirmed to be Cr_2Te_3 and $CrGeTe_3$ phases. The corresponding temperatures of the kinks are 60–70 K and 170–180 K, respectively, agreeing well with the T_c values of $CrGeTe_3$ and Cr_2Te_3. When $x \geq$ 0.6 mol, it is difficult to observe the two kinks in the M–T curves. It is well known that the temperature dependence of magnetic susceptibility $\chi(T)$ is usually plotted to verify the phase composition of a sample. The magnetic susceptibility χ follows the Curie–Weiss law: $\chi = M/H = C/(T - T_C)$, where M is the magnetization, H is the magnetic field strength, and C is the Curie temperature constant of a material. There is a linear relationship between $1/\chi$ and T for a specific material. The corresponding temperature is T_c when $1/\chi = 0$. Clearly, there are still two kink points between 70 and 200 K on the blue lines for both x = 0.6 and 0.8 mmol (Figures 3d and e), which represents two different phases. Only the fitted $1/\chi = T$ curve of x = 1.0 mmol is close to a straight line, and the corresponding temperature at $1/\chi = 0$ is approximately 67.5 K, close to the T_c value of $CrGeTe_3$ reported by C. Petrovic.[19] To conclude, the above M–T and $1/\chi = T$ curves further confirm the coexistence of hard Cr_2Te_3 and soft $CrGeTe_3$ phases during the cation exchange reaction.

We then applied TEM to investigate the structural characteristics of the transformation from the binary Cr_2Te_3 template to the ternary $CrGeTe_3$ nanostructure. A typical elemental mapping of the intermediate state with x = 0.4 mmol is shown in Figure 4a–c. In both regions A and B, the element distributions of Cr and Te are uniform, whereas the Ge is too sparse to be found. The atomic ratio is close to the stoichiometry of Cr_2Te_3, indicating that the main phase is Cr_2Te_3 in regions A and B. Region C exhibits a perfect hexagonal lattice with the distance between lines L_1 and L_3 of 0.683 nm (Figure 4d), consisting with its lattice constant (a) of

https://dx.doi.org/10.1021/jacs.9b13492
J. Am. Chem. Soc. 2020, 142, 4438–4444

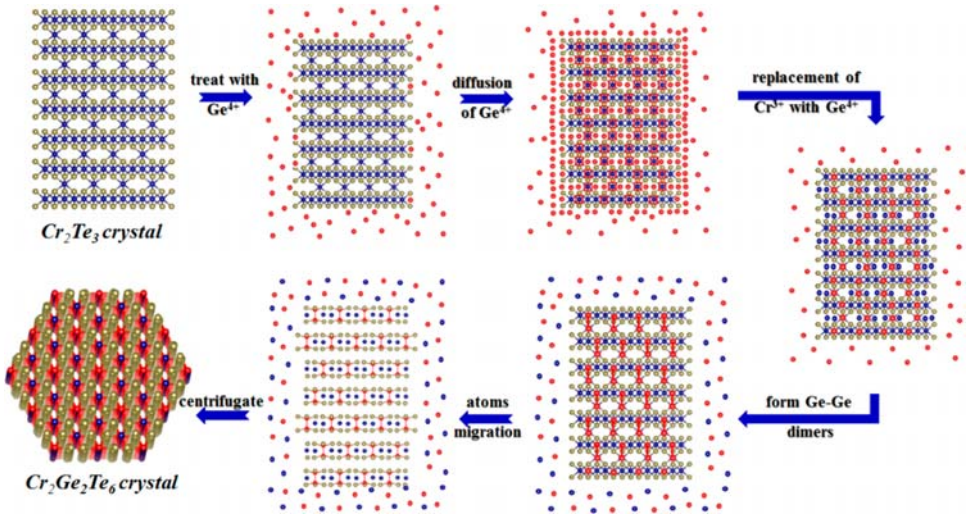

Figure 5. Schematic illustration of the cation exchange reaction process from non-vdW Cr_2Te_3 to vdW layered $CrGeTe_3$ nanosheets.

a $CrGeTe_3$ unit cell (inset of Figure 4d and Figure S4). Therefore, Cr_2Te_3 and $CrGeTe_3$ exist independently in the different regions, rather than growing with a heterojunction structure. Meanwhile, some Cr^{3+} cations in the Cr_2Te_3 lattice have been replaced by Ge^{4+} cations to form $CrGeTe_3$ fragments during the reaction process.

For the sample with x = 1.0 mmol, the products are mainly uniform hexagonal nanosheets with a diameter of about 1 μm and an average thickness of 60−70 nm (Figure S5a,b). When the sample was ultrasonically exfoliated in hexene for different time, the average thickness of the nanosheets was gradually reduced (Figure S5c−f). It is about 5−7 nm, which approximately equals 7−10 layers of $CrGeTe_3$ for the ultrasonic time of 2 h. The elements Cr, Ge, and Te are uniformly distributed in a single hexagonal nanosheet (Figure 4e−g) with an average atomic ratio of 1:1:3 (Figure S6b), in good agreement with the stoichiometric ratio of $CrGeTe_3$. Moreover, the atoms in region D (inset of Figure 4e) have a hexagonal close-packed (hcp) structure, and the in-plane lattice constant (a) is 0.683 nm (Figure 4h), indicating the pure phase of $CrGeTe_3$. Furthermore, the SAED pattern exhibits its single-crystal characteristics of a $CrGeTe_3$ nanosheet.

The chemical composition and valence of $CrGeTe_3$ (x = 1.0 mmol) are determined by high-resolution XPS survey (Figure 4i−k). The binding energies of both Cr-2p and Te-3d are very close to each other. Actually, the peaks located at 576.2 eV ($2p_{3/2}$) and 586.5 eV ($2p_{1/2}$) corresponds to Cr^{3+}, whereas the ones located at 572.3 eV ($3d_{5/2}$) and 582.6 eV ($3d_{3/2}$) belong to Te^{2-}.[32−34] It is impossible for Cr^0 and Te^{4+} to exist in $CrGeTe_3$ according to our simulated results. The two peaks at 29.7 eV (3d) and 32.1 eV (3d) in Figure 4k correspond to the binding energy of Ge^0 (Ge−Ge metal bond) and Ge^{4+} (Ge−Te covalent bond),[35] respectively, in agreement with our simulated results.

Furthermore, the reaction solutions were characterized by ICP (Figure S8). Sample I is the original reaction solution without any washing, and samples II−IV are the solutions after centrifugal washing for one, two, and three times in a hexane and ethanol mixed solvent. The concentration of Cr^{3+} is 1.18 g/kg in sample I, indicating that Cr^{3+} ions have been successfully replaced by Ge^{4+} during the reaction process. The concentration of Cr^{3+} in the solution decreases with the increase of washing times. Therefore, it can be speculated that the mechanism from non-vdW Cr_2Te_3 to vdW layered $CrGeTe_3$ follows the cation exchange reaction.[36]

The stability of 2D $CrGeTe_3$ nanosheets in ambient conditions is very crucial for practical applications.[37] We found there was no significant change for both the sample kept in air for 6 months and the one annealed at 300 °C for half an hour in a vacuum according to the XRD patterns (Figure S9a). Similar results were also observed in M−H curves (Figure S9b), demonstrating the robust stability after exposing in air or annealing under vacuum. Such excellent stability of 2D $CrGeTe_3$ nanosheets can be attributed to its intrinsic stability.[15] Meanwhile, the small organic ligands wrapped around the $CrGeTe_3$ might further enhance its oxidation resistance.

Finally, the above combined theoretical and experimental results allow us to present a picture for the transition from non-vdW Cr_2Te_3 to vdW layered $CrGeTe_3$ (Figure 5). The cation exchange reaction process can be divided into the following steps: (i) the diffusion of Ge^{4+} into the Cr_2Te_3 lattice, (ii) the substitution of Cr^{3+} by Ge^{4+}, and (iii) the emigration of Cr^{3+}. Specifically, when non-vdW Cr_2Te_3 nanosheets were treated with GeI_4 at a high temperature, the high concentration of Ge^{4+} ions easily and rapidly diffuse into layers with many Cr vacancies in the Cr_2Te_3 lattice (stage 1). Due to the lower formation energy of $CrGeTe_3$ (Figure 1), Ge^{4+} will sequentially replace Cr_{II} and Cr_{III} in Cr_2Te_3 to form $CrGeTe_3$ according to our calculation results. Meanwhile, these replaced Ge atoms prefer to form a Ge−Ge dimer, and some distortion of Te atoms occurs to reach the lowest energy and the most stable structure (stage 2). The partial replacement of Cr^{3+} with Ge^{4+} leads to the coexistence of the Cr_2Te_3 phase and the $CrGeTe_3$ phase due to the exfoliation between the layers. Finally, the substituted Cr^{3+} cations will move out from the $CrGeTe_3$ lattice (stage 3). After cation exchange, the stacking mode of $CrGeTe_3$ is ABCABC, rather than ABABAB in Cr_2Te_3. This is because the layered structure makes the crystal plane slip easily. Note that this cation exchange reaction is carried out only at approximately 350 °C, much lower than the growth temperature of $CrGeTe_3$

https://dx.doi.org/10.1021/jacs.9b13492
J. Am. Chem. Soc. 2020, 142, 4438−4444

single crystals. Therefore, this is a facile bottom-up chemical synthesis method for $CrGeTe_3$ 2D nanosheets.

4. CONCLUSIONS

In summary, high-quality 2D ferromagnetic vdW $CrGeTe_3$ nanosheets were synthesized from the non-vdW Cr_2Te_3 template through a bottom-up chemical cation exchange process. The theoretical calculation indicated that the cation exchange in the Cr_2Te_3 lattice is initiated from the Cr atoms surrounded by fewer Te atoms. This was due to their smaller steric hindrance and lower energy barrier. The Cr_2Te_3 hard magnetic phase can be completely transformed to the $CrGeTe_3$ soft magnetic phase when half of the Cr^{3+} cations were substituted by Ge^{4+}. The hard Cr_2Te_3 and soft $CrGeTe_3$ can exist separately during the cation exchange process. The as-prepared $CrGeTe_3$ nanosheets exhibited a uniform hexagon with a diameter larger than 1 μm and displayed a robust stability. Our work may speed up the investigation of 2D $CrGeTe_3$ with unique intrinsic long-range ferromagnetic order, while providing a novel approach to synthesize 2D nanosheets from a non-vdW template.

■ ASSOCIATED CONTENT

Supporting Information

The Supporting Information is available free of charge at https://pubs.acs.org/doi/10.1021/jacs.9b13492.

Supplementary figures and explanations (PDF)

■ AUTHOR INFORMATION

Corresponding Authors

Fang Wang − *School of Chemistry and Materials Science of Shanxi Normal University & Key Laboratory of Magnetic Molecules and Magnetic Information Materials of Ministry of Education, Linfen 041004, China; Research Institute of Materials Science of Shanxi Normal University & Collaborative Innovation Center for Shanxi Advanced Permanent Magnetic Materials and Technology, Linfen 041004, China;* orcid.org/0000-0003-3567-9108; Email: wf_0716@163.com

Ding-Jiang Xue − *Beijing National Laboratory for Molecular Sciences (BNLMS), CAS Key Laboratory of Molecular Nanostructure and Nanotechnology, Institute of Chemistry, Chinese Academy of Sciences, Beijing 100190, China;* orcid.org/0000-0002-7599-0008; Email: djxue@iccas.ac.cn

Xiaohong Xu − *School of Chemistry and Materials Science of Shanxi Normal University & Key Laboratory of Magnetic Molecules and Magnetic Information Materials of Ministry of Education, Linfen 041004, China; Research Institute of Materials Science of Shanxi Normal University & Collaborative Innovation Center for Shanxi Advanced Permanent Magnetic Materials and Technology, Linfen 041004, China;* orcid.org/0000-0001-7588-4793; Email: xuxh@sxnu.edu.cn

Authors

Huan Yang − *School of Chemistry and Materials Science of Shanxi Normal University & Key Laboratory of Magnetic Molecules and Magnetic Information Materials of Ministry of Education, Linfen 041004, China; Research Institute of Materials Science of Shanxi Normal University & Collaborative Innovation Center for Shanxi Advanced Permanent Magnetic Materials and Technology, Linfen 041004, China*

Huisheng Zhang − *Research Institute of Materials Science of Shanxi Normal University & Collaborative Innovation Center for Shanxi Advanced Permanent Magnetic Materials and Technology, Linfen 041004, China;* orcid.org/0000-0001-7369-9068

Lihong Guo − *School of Chemistry and Materials Science of Shanxi Normal University & Key Laboratory of Magnetic Molecules and Magnetic Information Materials of Ministry of Education, Linfen 041004, China*

Liyan Hu − *School of Chemistry and Materials Science of Shanxi Normal University & Key Laboratory of Magnetic Molecules and Magnetic Information Materials of Ministry of Education, Linfen 041004, China; Research Institute of Materials Science of Shanxi Normal University & Collaborative Innovation Center for Shanxi Advanced Permanent Magnetic Materials and Technology, Linfen 041004, China*

Lanfang Wang − *School of Chemistry and Materials Science of Shanxi Normal University & Key Laboratory of Magnetic Molecules and Magnetic Information Materials of Ministry of Education, Linfen 041004, China; Research Institute of Materials Science of Shanxi Normal University & Collaborative Innovation Center for Shanxi Advanced Permanent Magnetic Materials and Technology, Linfen 041004, China*

Complete contact information is available at: https://pubs.acs.org/10.1021/jacs.9b13492

Notes

The authors declare no competing financial interest.

■ ACKNOWLEDGMENTS

This work was supported by the National Key R&D Program of China (2017YFB0405703), National Natural Science Foundations of China (51971122, 51571135, 61434002, 51871137, 11804210, 21922512, and 21875264), and the Youth Innovation Promotion Association CAS (2017050).

■ REFERENCES

(1) Novoselov, K. S.; Geim, A. K.; Morozov, S. V.; Jiang, D.; Zhang, Y.; Dubonos, S. V.; Grigorieva, I. V.; Firsov, A. A. Electric field effect in atomically thin carbon films. *Science* **2004**, *306*, 666.

(2) Han, W.; Kawakami, R. K.; Gmitra, M.; Fabian, J. Graphene spintronics. *Nat. Nanotechnol.* **2014**, *9*, 794.

(3) Manzeli, S.; Ovchinnikov, D.; Pasquier, D.; Yazyev, O. V.; Kis, A. 2D Transition Metal Dichalcogenides. *Nat. Rev. Mater.* **2017**, *2*, 17033.

(4) Burch, K. S.; Mandrus, D.; Park, J. Magnetism in Two-Dimensional van Der Waals Materials. *Nature* **2018**, *563*, 47.

(5) Liu, S. C.; Yang, Y.; Li, Z. B.; Xue, D. J.; Hu, J. S. GeSe thin-film solar cells. *Mater. Chem. Front.* **2020**, DOI: 10.1039/C9QM00727J.

(6) Gong, C.; Zhang, X. Two-dimensional magnetic crystals and emergent heterostructure devices. *Science* **2019**, *363*, 706.

(7) Dietl, T. A ten-year perspective on dilute magnetic semiconductors and oxides. *Nat. Mater.* **2010**, *9*, 965.

(8) Zhou, Y.; Wang, Z.; Yang, P.; Zu, X.; Yang, L.; Sun, X.; Gao, F. Tensile strain switched ferromagnetism in layered NbS_2 and $NbSe_2$. *ACS Nano* **2012**, *6*, 9727.

(9) Zhang, Z.; Zou, X.; Crespi, V. H.; Yakobson, B. I. Intrinsic magnetism of grain boundaries in two-dimensional metal dichalcogenides. *ACS Nano* **2013**, *7*, 10475.

(10) Cao, T.; Li, Z.; Louie, S. G. Tunable magnetism and half-metallicity in hole-doped monolayer GaSe. *Phys. Rev. Lett.* **2015**, *114*, 236602.

(11) Sivadas, N.; Daniels, M. W.; Swendsen, R. H.; Okamoto, S.; Xiao, D. Magnetic ground state of semiconducting transition-metal trichalcogenide monolayers. *Phys. Rev. B: Condens. Matter Mater. Phys.* **2015**, *91*, 235425.
(12) Huang, C.; Feng, J.; Wu, F.; Ahmed, D.; Huang, B.; Xiang, H.; Deng, K.; Kan, E. Toward intrinsic room-temperature ferromagnetism in two-dimensional semiconductors. *J. Am. Chem. Soc.* **2018**, *140*, 11519.
(13) Mounet, N.; Gibertini, M.; Schwaller, P.; Campi, D.; Merkys, A.; Marrazzo, A.; Sohier, T.; Castelli, I. E.; Cepellotti, A.; Pizzi, G.; Marzari, N. Two-dimensional materials from high throughput computational exfoliation of experimentally known compounds. *Nat. Nanotechnol.* **2018**, *13*, 246.
(14) Li, H.; Ruan, S.; Zeng, Y. J. Intrinsic Van Der Waals Magnetic Materials from Bulk to the 2D Limit: New Frontiers of Spintronics. *Adv. Mater.* **2019**, *31*, 1900065.
(15) Gong, C.; Li, L.; Li, Z.; Ji, H.; Stern, A.; Xia, Y.; Cao, T.; Bao, W.; Wang, C.; Wang, Y.; Qiu, Z. Q.; Cava, R. J.; Louie, S. G.; Xia, J.; Zhang, X. Discovery of intrinsic ferromagnetism in two-dimensional van der Waals crystals. *Nature* **2017**, *546*, 265.
(16) Li, X.; Yang, J. $CrXTe_3$ (X= Si, Ge) nanosheets: two dimensional intrinsic ferromagnetic semiconductors. *J. Mater. Chem. C* **2014**, *2*, 7071.
(17) Xing, W.; Chen, Y.; Odenthal, P. M.; Zhang, X.; Yuan, W.; Tang, S.; Song, Q.; Wang, T.; Zhong, J.; Jia, S. Electric field effect in multilayer $Cr_2Ge_2Te_6$: A ferromagnetic 2D material. *2D Mater.* **2017**, *4*, 024009.
(18) Tang, X.; Fan, D.; Peng, K.; Yang, D.; Guo, L.; Lu, X.; Dai, J.; Wang, G.; Liu, H.; Zhou, X. Dopant induced impurity bands and carrier concentration control for thermoelectric enhancement in p-type $Cr_2Ge_2Te_6$. *Chem. Mater.* **2017**, *29*, 7401.
(19) Liu, Y.; Petrovic, C. Critical behavior of quasi-two-dimensional semiconducting ferromagnet $Cr_2Ge_2Te_6$. *Phys. Rev. B: Condens. Matter Mater. Phys.* **2017**, *96*, 054406.
(20) Wang, Z.; Zhang, T.; Ding, M.; Dong, B.; Li, Y.; Chen, M.; Li, X.; Huang, J.; Wang, H.; Zhao, X.; Li, Y.; Li, D.; Jia, C.; Sun, L.; Guo, H.; Ye, Y.; Sun, D.; Chen, Y.; Yang, T.; Zhang, J.; Ono, S.; Han, Z.; Zhang, Z. Electric-field control of magnetism in a few-layered van der Waals ferromagnetic semiconductor. *Nat. Nanotechnol.* **2018**, *13*, 554.
(21) Wang, N.; Tang, H.; Shi, M.; Zhang, H.; Zhuo, W.; Liu, D.; Meng, F.; Ma, L.; Ying, J.; Zou, L.; Sun, Z.; Chen, X. Transition from ferromagnetic semiconductor to ferromagnetic metal with enhanced Curie temperature in $Cr_2Ge_2Te_6$ via organic ion intercalation. *J. Am. Chem. Soc.* **2019**, *141*, 17166.
(22) Lohmann, M.; Su, T.; Niu, B.; Hou, Y.; Alghamdi, M.; Aldosary, M.; Xing, W.; Zhong, J.; Jia, S.; Han, W.; Wu, R.; Cui, Y.; Shi, J. Probing Magnetism in Insulating $Cr_2Ge_2Te_6$ by Induced Anomalous Hall Effect in Pt. *Nano Lett.* **2019**, *19*, 2397.
(23) Han, M. G.; Garlow, J. A.; Liu, Y.; Zhang, H.; Li, J.; DiMarzio, D.; Knight, M. W.; Petrovic, C.; Jariwala, D.; Zhu, Y. Topological magnetic-spin textures in two-dimensional van der Waals $Cr_2Ge_2Te_6$. *Nano Lett.* **2019**, *19*, 7859.
(24) Liu, Y.; Petrovic, C. Anisotropic magnetic entropy change in $Cr_2X_2Te_6$ (X= Si and Ge). *Phys. Rev. Mater.* **2019**, *3*, 014001.
(25) Kresse, G.; Joubert, D. From ultrasoft pseudopotentials to the projector augmented-wave method. *Phys. Rev. B: Condens. Matter Mater. Phys.* **1999**, *59*, 1758.
(26) Zhang, H.; Qin, W.; Chen, M.; Cui, P.; Zhang, Z.; Xu, X. Converting a two-dimensional ferromagnetic insulator into a high-temperature quantum anomalous Hall system by means of an appropriate surface modification. *Phys. Rev. B: Condens. Matter Mater. Phys.* **2019**, *99*, 165410.
(27) Grimme, S. Semiempirical GGA-type density functional constructed with a long-range dispersion correction. *J. Comput. Chem.* **2006**, *27*, 1787.
(28) Wang, F.; Du, J.; Sun, F.; Sabirianov, R.; Al-Aqtash, N.; Sengupta, D.; Zeng, H.; Xu, X. Ferromagnetic Cr_2Te_3 nanorods with ultrahigh coercivity. *Nanoscale* **2018**, *10*, 11028.
(29) Liu, Y.; Liu, M.; Swihart, M. T. Shape Evolution of Biconcave Djurleite $Cu_{1.94}S$ Nanoplatelets Produced from $CuInS_2$ Nanoplatelets by Cation Exchange. *J. Am. Chem. Soc.* **2017**, *139*, 18598.
(30) Son, D. H.; Hughes, S. M.; Yin, Y.; Alivisatos, A. P. Cation exchange reactions in ionic nanocrystals. *Science* **2004**, *306*, 1009.
(31) Liu, Y.; Liu, M.; Yin, D.; Qiao, L.; Fu, Z.; Swihart, M. T. Selective cation incorporation into copper sulfide based nano-heterostructures. *ACS Nano* **2018**, *12*, 7803.
(32) Mora, N.; Cano, E.; Bastidas, J. M.; Almeida, E.; Puente, J. M. Characterization of passivated tinplate for food can applications. *J. Coat. Technol.* **2002**, *74*, 53.
(33) Battistoni, C.; Mattogno, G.; Paparazzo, E.; Ingo, G. M. X-ray photoelectron spectroscopy analysis of a Cr-CrO_x multilayer electro-galvanized coating. *Surf. Coat. Technol.* **2004**, *29*, 105.
(34) Bala, M.; Meena, R.; Gupta, S.; Pannu, C.; Tripathi, T. S.; Varma, S.; Tripathi, S. K.; Asokan, K.; Avasthi, D. K. Formation of nanodots and enhancement of thermoelectric power induced by ion irradiation in PbTe: Ag composite thin films. *Nucl. Instrum. Methods Phys. Res., Sect. B* **2016**, *379*, 36.
(35) Murphy, N. R.; Jones, J. G.; Jakubiak, R.; Grant, J. T.; Sun, L.; Shutthanandan, V.; Ramana, C. V. Correlation between optical properties and chemical composition of sputter-deposited germanium oxide (GeO_x) films (postprint). *Opt. Mater.* **2014**, *36*, 1177.
(36) Liu, Y.; Yin, D.; Swihart, M. T. Valence selectivity of cation incorporation into covellite CuS nanoplatelets. *Chem. Mater.* **2018**, *30*, 1399.
(37) Yang, Y.; Liu, S. C.; Yang, W.; Li, Z.; Wang, Y.; Wang, X.; Zhang, S.; Zhang, Y.; Long, M.; Zhang, G.; Xue, D. J.; Hu, J. S.; Wan, L. J. Air-stable in-plane anisotropic $GeSe_2$ for highly polarization-sensitive photodetection in short wave region. *J. Am. Chem. Soc.* **2018**, *140*, 4150.

https://dx.doi.org/10.1021/jacs.9b13492
J. Am. Chem. Soc. 2020, 142, 4438−4444